# Near-field deformation of a liquid interface by atomic force microscopy

C. Mortagne,[1,2] V. Chireux,[1] R. Ledesma-Alonso,[3] M. Ogier,[1] F. Risso,[1] T. Ondarçuhu,[2] D. Legendre,[1] and Ph. Tordjeman[1,*]

[1]*IMFT - Université de Toulouse, CNRS-INPT-UPS, UMR 5502, 1 allée du Professeur Camille Soula, 31400 Toulouse, France*

[2]*Nanosciences Group, CEMES-CNRS, UPR 8011, 29 rue Jeanne Marvig, 31055 Toulouse cedex 4, France*

[3]*CONACYT -Universidad de Quitana Roo, Boulevar Bahía s/n,Chetumal, 77019, Quitana Roo, México*

(Received 3 April 2017; published 5 July 2017)

We experiment the interaction between a liquid puddle and a spherical probe by Atomic Force Microscopy (AFM) for a probe radius $R$ ranging from 10 nm to 30 $\mu$m. We have developed a new experimental setup by coupling an AFM with a high-speed camera and an inverted optical microscope. Interaction force-distance curves (in contact mode) and frequency shift–distance curves (in frequency modulation mode) are measured for different bulk model liquids for which the probe-liquid Hamaker constant $H_{pl}$ is known. The experimental results, analyzed in the frame of the theoretical model developed in Phys. Rev. Lett. **108**, 106104 (2012) and Phys. Rev. E **85**, 061602 (2012), allow to determine the "jump-to-contact" critical distance $d_{\min}$ below which the liquid jumps and wets the probe. Comparison between theory and experiments shows that the probe-liquid interaction at nanoscale is controlled by the liquid interface deformation. This work shows a very good agreement between the theoretical model and the experiments and paves the way to experimental studies of liquids at the nanoscale.

DOI: 10.1103/PhysRevE.96.012802

## I. INTRODUCTION

When a liquid encounters a solid or another liquid, it undergoes a jump-to-contact instability due to van der Waals (vdW) interactions between the two media. This phenomenon is crucial in coalescence of drops and in many situations where liquids are projected on solid surfaces. The jump-to-contact instability occurs at the nanoscale and results of the local liquid deformation. It is characterized by a threshold distance $d_{\min}$ below which the liquid wets the solid surface or forms an irreversible capillary bridge with a second liquid. To experiment the jump-to-contact instability, a nanoscale technique is necessary to probe the near field interaction force and to determine the $d_{\min}$ length. While Atomic Force Microscopy (AFM) has been developed to perform experiments in air [1] with unprecedented resolution for the characterization of solids, the study of liquids with AFM is still not often addressed in the literature [2–4] and provides new advances in particular in biophysics [5,6] and wetting [7,8].

Evaporation-condensation, electrical charges at the liquid surface, and liquid spreading during experiments may restrict the use of AFM. In particular, the study of liquids with low viscosity is challenging because the tip undergoes the liquid attraction and the jump-to-contact instability is uncontrolled. To study the near field interaction between a liquid and a probe with a nanoscale resolution, a new experimental setup must be developed to achieve AFM experiments. The AFM can be operated in two modes, the contact mode and the intermittent mode [9,10]. In the first one, the cantilever deflection is measured when the probe approaches the sample. After calibration, the probe-sample interaction force can be plotted versus the displacement. In the intermittent mode, two typical experiments called Amplitude Modulation-AFM (AM-AFM) and Frequency Modulation-AFM (FM-AFM) can be conducted: in the first experiments, the cantilever is vibrated close to the resonance frequency and the amplitude is measured versus the probe-sample displacement; in the second, the cantilever oscillates at a fixed resonance amplitude and the shift resonance frequency is measured versus the probe-sample displacement. A Phase Lock Loop (PLL) is used to maintain the oscillation phase of the cantilever at the resonance when the probe approaches the sample, the probe-sample interaction force being responsible of a decreasing of the resonance frequency. In all modes, the analysis of the results requires a theoretical model, in particular to determine the origin of the probe displacement, which is initially unknown.

In this paper, we study experimentally the interaction between a spherical probe and model liquids at the nanoscale. The paper is organized as follows. In Sec. II, we recall the theoretical model that is used to analyze the AFM experiments. In Sec. III, we describe the experimental setup and the procedure to perform AFM measurements in contact and FM modes. In particular, a lateral observation of the probe-liquid system with a high-speed camera was implemented in the AFM for *in situ* optical observations. The results are presented and analyzed in Sec. IV. Taking into account the liquid deformation, we observe a very good agreement between experiments and numerical simulations. This work shows that the jump-to-contact threshold $d_{\min}$ can thus be determined by FM-AFM with good accuracy.

## II. THEORETICAL MODEL

Recently, we have developed a nano-hydrodynamic model that predicts the surface deformation of a liquid film in interaction with a nano-probe [11–14]. Liquid and probe interact through non-retarded vdW forces. The model determines the threshold distance $d_{\min}$ between the undeformed liquid surface and the bottom surface of a spherical probe, below which the jump-to-contact instability arises. This distance, which is a characteristic of the probe-liquid static interaction, depends mainly on the probe-liquid Hamaker constant $H_{pl}$ and on the probe radius $R$. It is calculated by solving numerically the modified Young-Laplace equation [11,15]

$$\Delta P \simeq 2\,\gamma\,\kappa + \Pi_{pl}, \tag{1}$$

*philippe.tordjeman@imft.fr

 

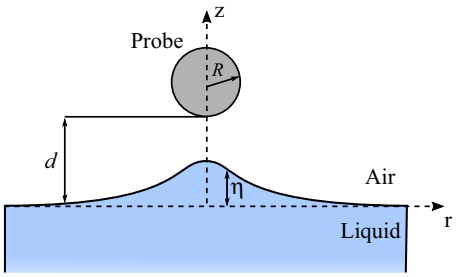


FIG. 1. Schema of the liquid deformation in interaction with a spherical probe. Parameters defined in the text.

where $\Delta P$ is the pressure difference across the liquid interface, $\gamma$ is the liquid-air surface tension, $\kappa$ is the local mean curvature, $\Pi_{pl}$ is the disjoining pressure associated with the probe-liquid interaction. The local mean curvature, expressed in axisymmetric cylindrical coordinates, takes the form

$$\kappa = -\frac{\partial}{2r\,\partial r}\left(r\frac{\partial \eta}{\partial r}\left[1+\left(\frac{\partial \eta}{\partial r}\right)^2\right]^{-1/2}\right), \tag{2}$$

where $\eta(r)$ is the local surface position (Fig. 1). The interaction potential corresponds to the potential energy difference between the perturbed state and the undisturbed original state. The disjoining pressure $\Pi_{pl}$ between the spherical probe and a given point of the liquid surface at $z = \eta$ is given by

$$\Pi_{pl} = -\frac{4H_{pl}R^3}{3\pi}\frac{1}{[(d+R-\eta)^2+r^2-R^2]^3}. \tag{3}$$

Here, $d$ is the separation distance between the unperturbed liquid interface and the probe bottom (Fig. 1). In this approach, the effects of gravity can be neglected due to the very low value of the Bond number, $B_o = R^2 g\Delta\rho/\gamma \simeq 10^{-7}$–$10^{-12}$, where $g$ and $\Delta\rho$ are the acceleration of gravity and the air/liquid density difference, respectively.

The theoretical value of $d_{\min}$ is obtained from the relationship between the probe displacement $d$ and the deformation $\eta_0$ of the liquid interface at $r = 0$ [12]:

$$d^* \simeq \eta_0^* + \sqrt{1+\left(\frac{H_a}{2C\,(\eta_0^*)^{3/2}}\right)^{1/3}} - 1, \tag{4}$$

where $d^* = d/R$ and $\eta_0^* = \eta_0/R$, $C = 0.4\,B_o^{0.06}/\sqrt{H_a}$, where $H_a = 4H_{pl}/(3\pi\gamma R^2)$ is the normalized Hamaker constant. At $d_{\min}$ the deformation is maximum and $\partial\eta_0^*/\partial d^* \to \infty$. In practice, we determine the maximum of $\eta_0$ by solving numerically $\partial d^*/\partial\eta_0^* = 0$, and $d_{\min}$ from Eq. (4) for the maximum of $\eta_0$. Typically, for a spherical probe in interaction with a bulk liquid with a Hamaker constant $H_{pl} \simeq 6\times10^{-20}$ J, $d_{\min}$ is found to vary between 2 and 30 nm when $R$ varies between 1 nm and 30 $\mu$m. The theoretical study of the liquid deformation in interaction with an oscillating spherical probe points out that the jump-to-contact instability occurs at a lower distance than $d_{\min}$ when the oscillation frequency is very large (of the order of $10^8$ Hz). On the other hand, for typical frequency of AM-AFM or FM-AFM experiments (between 1 and 500 kHz), the jump-to-contact instability occurs at distance close to $d_{\min}$ [14].

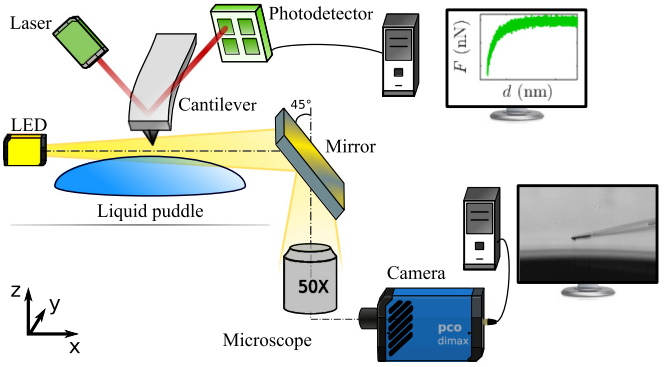


FIG. 2. Schema of the experimental setup: AFM coupled with a high-speed camera and an inverted optical microscope.

## III. AFM EXPERIMENTS

We investigate the interaction between spherical probes and model liquids at the nanoscale by means of an AFM. In this study, we consider four different model fluids, which are characterized by a same Hamaker constant $H_{pl} \simeq 6\times10^{-20}$ J [16,17]: diethylene glycol (2EG), triethylene glycol (3EG), tetraethylene glycol (4EG), and glycerine (Gly). The liquids are purchased from Sigma-Aldrich and are used as received. Their dynamic viscosity and surface tension are $\mu = 30, 40, 50,$ and 910 mPa s and $\gamma = 50, 48, 46,$ and 63 mN/m, respectively. As a consequence, the jump-to-contact instability involves a characteristic velocity $\gamma/\mu = 1.7$, 1.2, 0.9, and $7\times10^{-2}$ m/s, respectively. The time to wet the probe $d_{\min}\,\mu/\gamma$ is close to $8\times10^{-9}$ s for 2EG, 3EG and 4EG and $1\times10^{-7}$ s for Gly. Puddles of liquids are deposited on a glass slide that is cleaned just before AFM experiments.

A JPK Nanowizard 3 AFM is employed in contact and FM modes to measure the force curves and the frequency shift curves over a liquid puddle (Fig. 2). For FM experiments, the PLL device of the signal access module Vortis JPK operates the phase feedback. A specific cantilever holder has been built by JPK to perform experiments with liquids. It consists of a 45° gold mirror (NA 0.3) to observe the side view of the cantilever and a "direct drive" piezo transducer to vibrate the cantilever at a given amplitude and frequency. An inverted optical microscope Nikon Eclipse Ti is placed under the AFM. A 50 × /0.6 long distance objective is employed to visualize the liquid puddle-cantilever system before and during the experimental runs. A high-speed PCO Dimax Camera is coupled to the optical microscope. The camera is mounted with an air gap to prevent vibrations of the AFM. During the AFM experiments, the optical image is focused at the interface between the liquid and the probe. The maximum frame rate of the camera is 1279 fps for image size of 2016 × 2016 pixels. When the size is reduced to 300 × 300 pixels, the camera frame rate can reach 45 000 fps. The lighting is provided via an optical fiber bundle by a LED light source equipped with an infrared filter. The images are calibrated by means of a micron ruler. AFM and camera are synchronized via the signal access module. The coupling between AFM measurements and high-speed camera observations allows to ensure positioning of the probe over the puddle, to assess possible evaporation, and to observe the dynamics of the wetting process of the

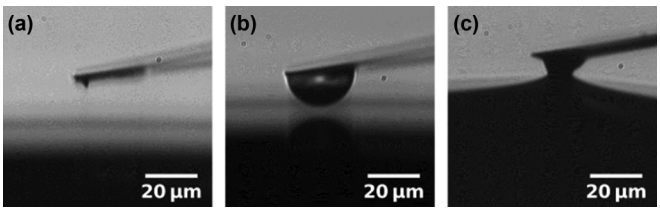


FIG. 3. Images of probes recorded by a high-speed camera over a Gly puddle: (a) Nanometric probe (AppNano Hydra); (b) Gly droplet probe; (c) Wetting of a probe (PPP Nanosensors) after jump-to-contact.

cantilever-probe system after the jump-to-contact (Fig. 3). We verified from the camera images that no evaporation takes place during the AFM measurements.

Whereas the Hamaker constant of standard liquids belongs to a single decade ($10^{-19}$ J $\leqslant H_{pl} \leqslant 10^{-20}$ J), the probe radius $R$ may spread over several decades. $R$ is therefore the main parameter that controls the amplitude of the probe-liquid interaction forces and thus that determines the range of interaction. In this study, we use different cantilevers with different tip radii, which varies over five decades, from $10^{-9}$ to $10^{-4}$ m. The tip radii are measured by SEM observations, after the usual cantilever calibration procedure carried out before each AFM measurement. To obtain probes with a radius larger than 1 $\mu$m, we have developed a method to deposit a small drop at the cantilever extremity. The droplet is maintained by the wetting force between the liquid and the cantilever, and its size depends on the liquid volume that has been transferred to the cantilever. The droplet is small enough to remain spherical by surface tension, so that it can be considered as a rigid spherical probe. The probe radius is measured on microscopy camera images just before each AFM experiment. It has been checked that the values of $R$ measured by optical microscopy are closed to those calculated with the resonance frequency shift resulting of the additional mass induced by the liquid at the extremity of the cantilever.

For contact mode experiments, two different cantilevers are used: (1) Hydra 6V-200WG AppNano with a $k = 0.12$ N/m and a radius $R \simeq 25$ nm; (2) colloïdal PT-SiO2.Si.1 Novascan with $k = 0.58$ N/m and $R \simeq 450$ nm. For FM-AFM experiments, three different cantilevers are used: (1) PPP-NCHAuD Nanosensors with $k = 31$ N/m and $R = 12$ nm; (2) the same model with $k = 31$ N/m and $R = 45$ nm; (3) PT-SiO2.Si.1 Novascan with $k = 19.5$ N/m and $R = 450$ nm. The cantilever stiffnesses are characterized by thermal noise using the deflection sensitivity derived from contact mode experiments on a silicon wafer substrate [18]. Note that the stiffness of all the present cantilevers is at least four times larger than the effective spring constant of the interface, which is of the order of $\gamma/2$ [19]. Therefore, the jump-to-contact is not a consequence of a mechanical instability of the cantilever, but is the result of an hydrodynamic instability of the liquid interface. This is confirmed by the inspection of the video records. In contact and FM-AFM modes the force $F$ and the frequency shift $\Delta f$ are plotted versus the probe-liquid distance $d$. The latter is calculated by the difference between the piezo elevation $z$ and the cantilever deflection.

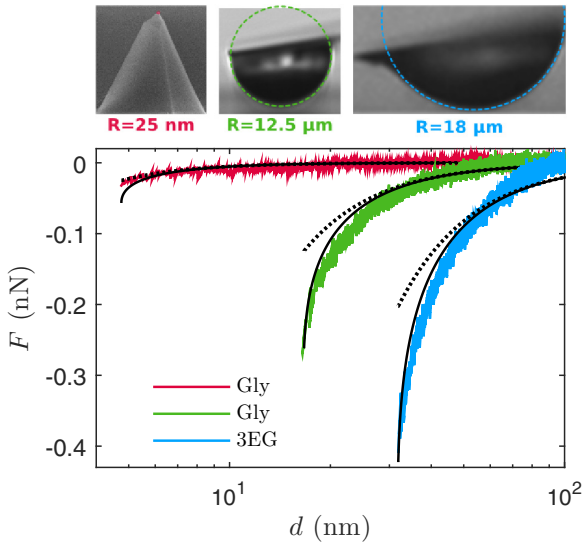


FIG. 4. Probe-liquid interaction force vs probe displacement. The experimental curves (solid colored lines) are fitted with Eq. (6) (solid black lines) and Eq. (7) (dotted lines).

More than 100 experimental runs have been performed. However, a quantitative assessment of the reproducibility of the experiments was not possible since the probe-liquid system is modified after each AFM experiment due to the irreversible wetting of the probe. Nevertheless, it has been checked that experiments realized with probes having similar characteristics yielded to similar results. All the AFM experiments are realized in a gray room maintained at a constant temperature of $23 \pm 1\,^{\circ}$C.

Figure 3 displays three images of cantilevers in interaction with a Gly puddle, before and after the jump-to-contact instability. In Fig. 3(a), the probe consists of the tip of a Hydra cantilever whereas, Fig. 3(b) shows a probe that consists of a small Gly droplet attached to the tip. With the present lighting conditions, interference fringes are observed at the puddle surface. For instance, Fig. 3(c) displays an image extracted from a high-speed movie during the wetting of a PPP tip. In Figs. 4 and 6, equivalent spheres estimated by SEM and optical microscopy (dashed lines) are superimposed onto images of some probes.

## IV. RESULTS AND DISCUSSION

### A. Experiments in contact mode

In a first set of experiments, we carried out force-displacement curves in contact mode. As an example, three typical curves are shown in Fig. 4 for $R \simeq 25$ nm, 12 $\mu$m, and 18 $\mu$m with Gly and 3EG. The probe velocity is 100 nm/s$^{-1}$. For a nanometer-sized probe, the results point out that the probe-liquid interaction is characterized by small magnitude and a short range. The maximum force, which is obtained for $d \simeq d_{\min}$, is of the order of $5 \times 10^{-11}$ N, close to the limit of detection of the AFM. For a micrometer-sized probe, a much larger maximum force is measured, in between 2 to $4 \times 10^{-10}$ N.

Following the approach of [20], the experimental curves can be fitted with the vdW force $F_{\mathrm{vdW}}$ between a deformable

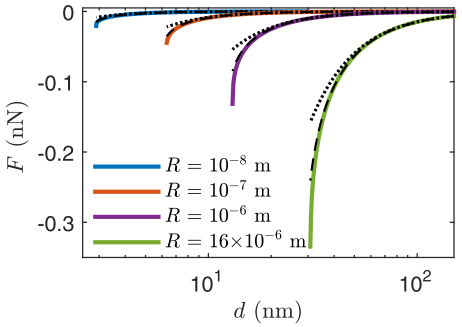


FIG. 5. Theoretical probe-liquid interaction force vs probe displacement calculated with Eq. (5) (solid lines), Eq. (6) (dashed line), and Eq. (7) (dotted lines) for four different probe radii.

liquid interface and a sphere of radius $R$:

$$F_{\mathrm{vdW}} = \frac{8\,H_{pl}R^3}{3}\int_0^{\infty}\frac{r\,dr}{([d+R-\eta(r)]^2+r^2-R^2)^3}. \quad (5)$$

The force takes into account the interface deformation $\eta(r)$, which can be calculated numerically from the model recalled in Sec. II. Considering that most of the interaction force comes from the region around $r = 0$, we can assume that

$$F_{\mathrm{vdW}} \simeq \frac{4H_{pl}R^3}{6[d-\eta_0(d)]^2[d-\eta_0(d)+2R]^2}, \quad (6)$$

where $\eta_0(d)$ is calculated from Eq. (4). Figure 5 compares the exact expression of $F_{\mathrm{vdW}}$ [Eq. (5)] with its approximate expression [Eq. (6)] for four different probe radii.

It is clear that the force mainly depends upon the maximum liquid deformation at $r = 0$ and that it is therefore relevant to fit the experimental results by Eq. (6) in order to determine the value of $R$. However, even though Eq. (6) predicts the correct shape of the interaction force, it underestimates the value of the maximum force compared to the result obtained with the exact expression of $F_{\mathrm{vdW}}$.

Figure 5 also compares Eq. (5) to the vdW force calculated by neglecting the surface deformation,

$$F'_{\mathrm{vdW}} \simeq \frac{4H_{pl}R^3}{6d^2(d+2R)^2}. \quad (7)$$

These results show that the interface deformation plays a crucial role in the probe-liquid interaction and hence cannot be neglected. The magnitude of the exact interaction force $F_{\mathrm{vdW}}$ indeed becomes significantly larger than $F'_{\mathrm{vdW}}$ when the probe-liquid distance approaches $d_{\mathrm{min}}$.

The experimental curves are fitted by adjusting the sphere radius $R$ which minimizes the standard deviation between the experimental curves and Eq. (6). Then, the value of $d_{\mathrm{min}}$ is calculated from Eq. (4), which allows to determine the origin of the probe displacement. We observe that $d_{\mathrm{min}}$ increases by more than one order of magnitude when the radius increases from 25 nm to 16 $\mu$m. For all experiments, the Hamaker constant is fixed to $H_{pl} = 6\times10^{-20}$ J, which is a reasonable value for the present probes and liquids. Using the model of Israelachvili of composition of Hamaker constants [17], we checked that $H_{pl}$ is indeed in between $5\times10^{-20}$ J and $1\times10^{-19}$J whatever the probe composition [21].

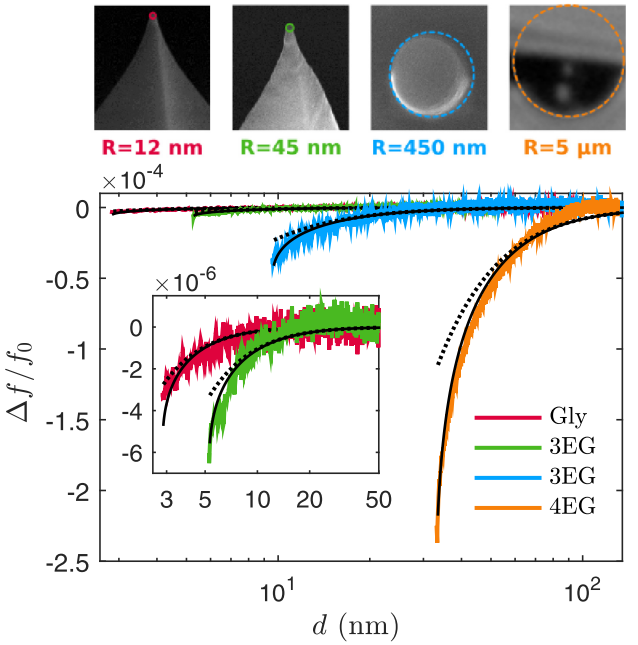


FIG. 6. Normalized frequency shift $\Delta f/f_0$ vs probe displacement $d$. The experimental curves (solid colored lines) are fitted with Eq. (8) combined with Eq. (6) (solid black lines) and Eq. (7) (dotted lines).

The fits obtained in Fig. 4 give $R \simeq 55$ nm, 3 $\mu$m, and 22 $\mu$m compared to $R \simeq 25$ nm, 12 $\mu$m, and 18 $\mu$m measured by SEM and optical microscopy. We observe a satisfactory agreement between the experimental curves and the model Eq. (6). In Fig. 4, $F'_{\mathrm{vdW}}$ is also plotted for the same fitted radii. The comparison with the experimental results shows clearly that the interface deformation has to be taken into account, which is consistent with the conclusions drawn from Fig. 5. The discrepancy between the values of $R$ fitted by means of the theory and those measured by microscopy is mainly due to the fact that the value of $H_{pl}$ is not known with a sufficient accuracy. Also, the values of $R$ measured by microscopy have been obtained by assuming that the probe is spherical. This assumption does not take into account the real tip and cantilever geometries. Moreover, for large values of $R$, the droplets may slightly deform during the experiments, which can induce a change in the probe curvature.

### B. Experiments in FM mode

In a second time, FM-AFM experiments are performed with 2EG, 3EG, 4EG, and Gly. Figure 6 presents selected shift-frequency curves obtained with $R \simeq 12$ nm, 45 nm, 450 nm, and 12 $\mu$m. This mode is able to make a clear distinction between the probe-liquid interactions for $R \simeq 12$ nm and $R \simeq 45$ nm. In contrast with contact mode, FM-AFM is accurate enough to characterize the interaction for $R < 100$ nm. This is made possible thanks to the PPL control and to the great sensitivity of the frequency shift to the probe-liquid distance, which is related to the force gradient. In this mode, $d_{\mathrm{min}}$ is detected when the phase of the cantilever oscillations and the gain of the AFM actuator both diverge. As in contact mode, the value of $R$ is obtained by fitting the experimental curves with a theoretical model by the least square method.

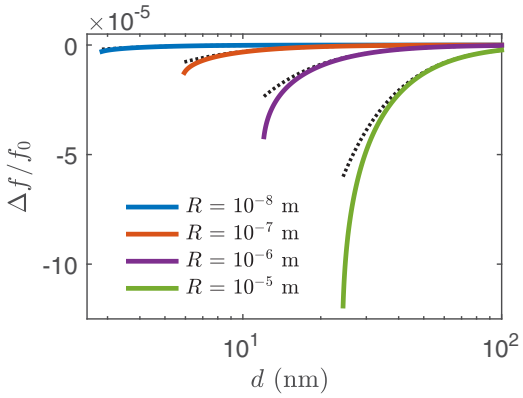


FIG. 7. Theoretical normalized frequency shift vs probe displacement, calculated with Eq. (8) combined with Eqs. (6) (solid line) and (7) (dotted lines) for five different probe radii.

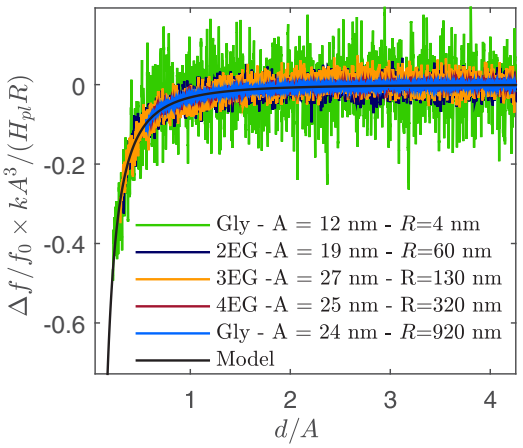


FIG. 8. Master curve of the normalized frequency shift as a function of the normalized displacement for five experimental conditions. $R$ and $d_{\min}$ are obtained by fitting the experimental results with Eq. (9)

Following the approach of Giessibl [22] and Hölscher [23] for FM-AFM experiments on solid surfaces, the theoretical expression of $\Delta f$ is given by

$$\frac{\Delta f}{f_0} = -\frac{1}{2\pi k A}\int_0^{2\pi} F_{vdW}(x)\cos(x)\,\mathrm{d}x, \qquad (8)$$

where $f_0$ is the cantilever eigenfrequency and $A$ is the oscillation amplitude. In this relationship, $\Delta f$ is a function of the liquid deformation $\eta_0(d)$. Now, $d$ is the minimum distance between the probe and the undeformed liquid surface that is reached during an oscillation, and $d + A$ is the mean position of the cantilever. Here, $d_{\min}$ is calculated by means of Eq. (4) from the fitted value of $R$. The fitting curves are presented in Fig. 6. The fitted values are $R \simeq 12$ nm, 66 nm, 470 nm, and 27 $\mu$m compared to $R \simeq 12$ nm, 45 nm, 450 nm, and 12 $\mu$m measured by microscopy. The corresponding values of $d_{\min}$, calculated by numerical simulations, are $d_{\min} = 2.8$ nm, 5.3 nm, 9.6 nm, and 33.1 nm, respectively.

In the limit of accuracy of the method, we observe a remarkable agreement between the experiments and the model that takes into account the maximal deformation of the liquid interface [Eqs. (6) and (8)]. The results obtained in the FM-AFM mode confirm that the liquid deformation plays a crucial role, especially when the distance of the oscillating probe approaches $d_{\min}$.

### C. Liquid deformation for $R \lesssim 1$ $\mu$m

Figure 7 compares the theoretical frequency shift obtained by accounting for the liquid deformation [Eqs. (6) and (8)] and without accounting for the liquid deformation [Eqs. (7) and (8)] for $R$ ranging from $10^{-9}$ m to $10^{-5}$ m. It turns out that the deformation plays a significant role only for $R$ larger than 1 $\mu$m.

Neglecting the deformation and assuming $d \lesssim R$, an explicit analytic expression of the frequency shift can be derived from Eqs. (7) and (8),

$$\frac{\Delta f}{f_0}\frac{kA^3}{H_{pl}R} = -\frac{1}{6\left[(d/A+1)^2-1\right]^{3/2}}. \qquad (9)$$

Hence, for $R \lesssim 1$ $\mu$m, the normalized experimental frequency shifts of all systems should gather on a master curve according to Eq. (9). Figure 8 presents the evolution of the experimental normalized frequency, $\frac{\Delta f}{f_0}\frac{kA^3}{H_{pl}R}$, as a function of the normalized distance, $d/A$, for five different systems with $R$ ranging from 4 to 920 nm and $A$ ranging from 12 to 27 nm. The master curve of Fig. 8 confirms that the liquid deformation can be neglected in FM mode for $R < 1$ $\mu$m. Note that the apparent noise in the master curve comes from the normalization in $A^3/R$, which exacerbates the experimental noise for small radii.

Finally, we consider the relationship between $d_{\min}$ and $R$. We have carried out more than 100 experiments in FM-AFM with all the liquids. As we dispose of a limited number of cantilevers, we developed a protocol to change the probe radius by successive wetting of AFM tips. In this way, we produced probes with radii ranging from $10^{-9}$ to $10^{-5}$ m. $R$ and $d_{\min}$ are determined by fitting the experimental curves with Eq. (9). Note that $d_{\min}$ and $R$ are two parameters that are adjusted when fitting by Eq. (9), $d_{\min}$ is thus not derived from $R$ by using Eq. (4). It is worth mentioning that the liquid deformation is not taken into account since most of the experiments are performed with probes with radii smaller than 1 $\mu$m. This approximation is strengthened by the results presented in Fig. 9.

The symbols in Fig. 9(a) show the experimental evolution of $d_{\min}$ over four decades of $R$ for the four studied liquids. It turns out that the jump-to-contact instability occurs at a distance of the order of $R$ for $R \sim 10^{-9}$ m, but at a distance a thousand times smaller than $R$ when $R$ is of the order of one micrometer. The theoretical predictions derived from Eq. (4) are represented by plain lines. The agreement between the measurements and the theory is satisfactory if we consider that a single approximate value of the Hamaker constant has been used for all the liquids, which however have different surface tensions. The log-log representation puts into light a simple scaling, $d_{\min} \sim R^{1/3}$, which can be understood by assuming that the mechanical instability occurs when the gradient of the interaction force $H_{pl}R/d^3$ exceeds the interface stiffness $\gamma/2$.

Figure 9(b) presents the same results in an adimensional form, $d^*_{\min}$ vs $H_a$. Thanks to the normalization, the experimental values of $d^*_{\min}$, obtained for a range of $H_a$ that covers height decades from $10^{-8}$ to 1, all nicely gather on the master curve

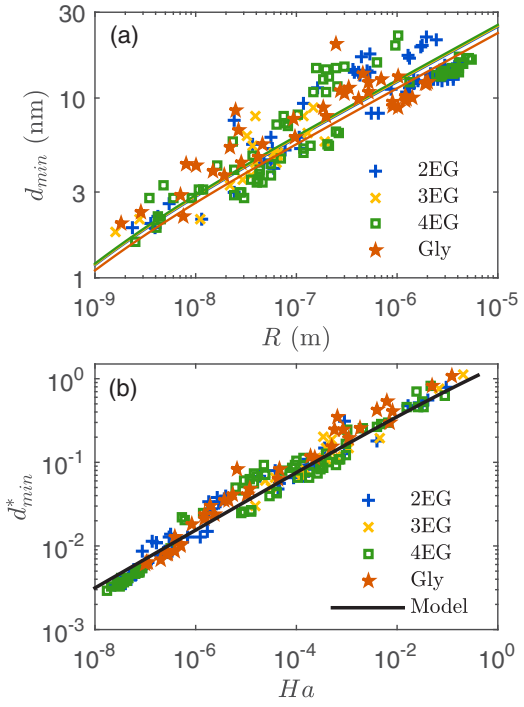


FIG. 9. Experimental and theoretical jump-to-contact threshold distance. (a) $d_{\min}$ vs probe radius $R$. The colored lines correspond to the model calculated for the different liquids (see Sec. II). (b) Non-dimensional distance $d^*_{\min}$ vs normalized Hamaker constant $H_a$. The data follow the empirical relation $d^*_{\min} \simeq 1.53 \times H_a^{1/3}$.

predicted by the model. From a practical point of view, the value of $d_{\min}$ for any liquids and sphere radii can be estimated with an error smaller than 7% by the following empirical correlation: $d^*_{\min} \simeq 1.53 \times H_a^{1/3}$.

## V. CONCLUSION

In this work, we have investigated the interaction between a spherical probe and a liquid puddle composed of several model liquids by means of AFM for probe radii spreading over five decades. The development of a new experimental AFM setup enables the study of the interaction between a liquid and a probe at nanoscale. The coupling between AFM measurements and side-view observations with a high-speed camera permits the positioning of the probe over the puddle, the measurement of the probe radius just before AFM experiments, and the description of the wetting dynamics of the cantilever-probe system after the jump-to-contact. Moreover, monitoring with a fast camera allows to check whether the probe radius is affected by evaporation just before AFM experiments.

We found that the van der Waals interaction can be probed by FM-AFM experiments with a good accuracy. In particular, our technique allows to measure the jump-to-contact threshold distance $d_{\min}$. We found a remarkable agreement between the present experimental results and the theory that describes the interface deformation by a balance between vdW, capillary forces and gravity. We also showed that the liquid deformation has to be taken into account for large probe radii but can be neglected for $R \lesssim 1\,\mu$m. FM-AFM experiments allow to quantify the range of interaction between a liquid and a solid or between two liquids, and yield a simultaneous and independent determination of $H_{pl}$ and $R$.

In the continuation of this work, AFM can be used to characterize liquids properties and to study the liquid dynamics at the nanoscale. This requires to conduct AFM experiments in non-contact mode at distance larger than $d_{\min}$. Surface migration of surfactants, topography of nanostructured liquids, nucleation and growth of instabilities, nucleation of vortex structures, and surface charge distribution of conducting liquids are example of phenomena that could be investigated.

## ACKNOWLEDGMENTS

The authors thank the JPK Company which has accepted to develop a new cantilever holder with a lateral side view mirror for FM-AFM experiments. The authors also thank S. Cazin and M. Marchal for their implication in the setup development. This study has been partially supported through the ANR by the NANOFLUIDYN project (grant no. ANR-13-BS10-0009).

[1] G. Binnig, C. F. Quate, and C. Gerber, Phys. Rev. Lett. **56**, 930 (1986).
[2] A. Checco, H. Schollmeyer, J. Daillant, P. Guenoun, and R. Boukherroub, Langmuir **22**, 116 (2006).
[3] A. Checco, Y. Cai, O. Gang, and B. M. Ocko, Ultramicroscopy **106**, 703 (2006).
[4] T. Ondarçuhu and J.-P. Aimé, *Nanoscale Liquid Interfaces: Wetting, Patterning and Force Microscopy at the Molecular Scale* (Pan Stanford Publishing, Singapore, 2013).
[5] E. Canetta, A. Duperray, A. Leyrat, and C. Verdier, Biorheology **42**, 321 (2005).
[6] O. Chaudhuri, S. H. Parekh, W. A. Lam, and D. A. Fletcher, Nature Methods **6**, 383 (2009).
[7] T. Pompe and S. Herminghaus, Phys. Rev. Lett. **85**, 1930 (2000).
[8] J. Becker, G. Grün, R. Seemann, H. Mantz, K. Jacobs, K. R. Mecke, and R. Blossey, Nat. Mater. **2**, 59 (2003).
[9] F. J. Giessibl, Rev. Mod. Phys. **75**, 949 (2003).
[10] R. Garcıa and R. Perez, Surf. Sci. Rep. **47**, 197 (2002).
[11] R. Ledesma-Alonso, D. Legendre, and P. Tordjeman, Phys. Rev. Lett. **108**, 106104 (2012).
[12] R. Ledesma-Alonso, P. Tordjeman, and D. Legendre, Phys. Rev. E **85**, 061602 (2012).
[13] R. Ledesma-Alonso, D. Legendre, and P. Tordjeman, Langmuir **29**, 7749 (2013).
[14] R. Ledesma-Alonso, P. Tordjeman, and D. Legendre, Soft Matter **10**, 7736 (2014).
[15] D. B. Quinn, J. Feng, and H. A. Stone, Langmuir **29**, 1427 (2013).
[16] J. Visser, Adv. Colloid Interface Sci. **3**, 331 (1972).

[17] J. N. Israelachvili, *Intermolecular and Surface Forces* (Academic Press, New York, 2011).

[18] N. Burnham, X. Chen, C. Hodges, G. Matei, E. Thoreson, C. Roberts, M. Davies, and S. Tendler, Nanotechnology **14**, 1 (2002).

[19] J. Dupre de Baubigny, M. Benzaquen, L. Fabié, M. Delmas, J.-P. Aimé, M. Legros, and T. Ondarçuhu, Langmuir **31**, 9790 (2015).

[20] H. Hamaker, Physica **4**, 1058 (1937).

[21] Note, according to Israelachvili [17], the Hamaker constant $H_{132}$ of media 1 and media 2 interacting across medium 3 reads $H_{132} \sim (\sqrt{H_1} - \sqrt{H_3})(\sqrt{H_2} - \sqrt{H_3})$ where $H_i$ is the Hamaker constant of the media $i$. Considering that the Hamaker constant of air can be neglected compared to the Hamaker constants of the probe $H_p$, and the liquid $H_l$, $H_{pl}$ is simply given by $H_{pl} = \sqrt{H_p H_l}$. In this study we take $H_p = 1.9 \times 10^{-19}$ J for Si probes (Hydra and PPP), $H_p = 6.5 \times 10^{-20}$ J for $SiO_2$ probes (Novascan) and $H_l$ is comprised between 5 and $7 \times 10^{-20}$ J for liquids.

[22] F. J. Giessibl, Phys. Rev. B **56**, 16010 (1997).

[23] H. Hölscher, U. Schwarz, and R. Wiesendanger, Appl. Surf. Sci. **140**, 344 (1999).